Inorganic Chemistry

Article

pubs.acs.org/IC

Spectroscopic and Phosphorescent Modulation in Triphosphine-Supported $PtAg_2$ Heterotrinuclear Alkynyl Complexes

Li-Yi Zhang, Liang-Jin Xu, Xu Zhang, Jin-Yun Wang, Jia Li, and Zhong-Ning Chen*

State Key Laboratory of Structural Chemistry, Fujian Institute of Research on the Structure of Matter, Chinese Academy of Sciences, Fuzhou, Fujian 350002, China

Supporting Information

ABSTRACT: A series of highly phosphorescent $PtAg_2$ heterotrinuclear alkynyl complexes with bis(diphenylphosphinomethyl)-phenylphosphine (dpmp) were prepared and characterized structurally. The solution phosphorescence with various emitting colors is systematically modulated by modifying substituents as well as π-conjugated systems in aromatic acetylides. The crystals, powders, or films exhibit reversible stimuli-responsive phosphorescence changes upon exposure to vapor of MeCN, pyridine, DMF, etc., resulting from perturbation of d^8-d^{10} metallophilic interaction in the excited states as a consequence of the formation/disruption of Ag−solvent bonds. Both experimental and time-dependent density functional theory (TD-DFT) studies demonstrate that d^8-d^{10} metallophilic interaction exerts a crucial role on phosphorescent characteristics due to the $PtAg_2$ cluster-based $^3[d \rightarrow p]$ state. This study affords a paradigm for phosphorescence modulation in d^8−d^{10} heteronuclear complexes.

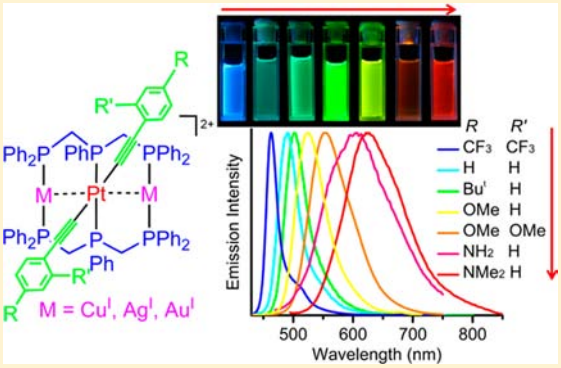

INTRODUCTION

Phosphorescent emission of transition metal complexes occurs mostly in coordination systems with d^6, d^8, or d^{10} metal ions.[1,2] Phosphorescent metal complexes with d^8 or d^{10} metal ions are particularly interesting because additional d^8-d^8 or d^{10}-d^{10} metallophilic interactions with the energy comparable to that of hydrogen bonds not only exert extra stability on the aggregate structures,[3] but also play a key role in determining the phosphorescent characteristic.[1,2] As strong-field ligands with comparable coordination capability, both acetylide and phosphine are facile for the coordination to d^8 or d^{10} metal ions,[1−3] resulting in largely raising the d-d state to relatively inaccessible energies so that an emissive triplet state is achieved. Although a limited number of d^8-d^{10} heterometallic complexes have been prepared,[4−26] few systematical studies on their photophysical properties have been performed.[9,10] In fact, systematic modulation of the phosphorescence properties relevant to d^8-d^{10} metallophilic interactions remains to be performed.

Herein, we focus on systematic modulation of spectroscopic and phosphorescence properties by the elaborate design of $PtAg_2$ heterotrinuclear alkynyl complexes using bis-(diphenylphosphinomethyl)phenylphosphine (dpmp) as a bridging ligand. These doubly dpmp-supported $PtAg_2$ alkynyl complexes exhibit mostly brilliant phosphorescence in both fluid solutions and solid states at ambient temperature. The solution phosphorescence with various visible emitting colors from the blue to the red spectral region is systematically modulated by not only introducing electron-donating or -withdrawing substituents, but also modifying π-conjugated system in aromatic acetylide ligands. They exhibit dramatic phosphorescence vaporchromism in the solid state upon exposure to vapor of MeCN, pyridine, or DMF having coordination character to metal ions. Both experimental and computational studies demonstrate that the $PtAg_2$ cluster-based $^3[d \rightarrow p]$ triplet excited state exerts a crucial role on the phosphorescent characteristics.

RESULTS AND DISCUSSION

Synthesis and Characterization. Initially, the reaction was performed by mixing equimolar *trans*-$Pt(PPh_3)_2(C{\equiv}CPh)_2$ with $[Ag_3(dpmp)_2](ClO_4)_3$[25,26] in CH_2Cl_2. The products were separated by silica gel column chromatography. While the first colorless band was identified as $[Ag(PPh_3)_4](ClO_4)$, yellow heterotrinuclear complex $[PtAg_2(dpmp)_2(C{\equiv}CPh)_2]](ClO_4)_2$ (**1**) was collected as the second band in 80% yield. Obviously, the formation of **1** is involved in the substitution of Pt-bound PPh_3 with P donors of dpmp. On the basis of the stoichiometric ratio of Pt/Ag/dmpm = 1: 2: 2 in complex **1**, the synthetic procedure was then optimized by mixing equiv. $Ag(tht)(ClO_4)$ and dpmp, followed by the addition of 0.5 equiv. $Pt(PPh_3)_2(C{\equiv}CPh)_2$. Complex **1** was indeed accessed in higher yield (85%) as expected. With this synthetic procedure, a series of $PtAg_2$ complexes (**1**−**9**, Scheme 1) with various substituents in aromatic acetylides were thus

Received: January 8, 2013
Published: April 12, 2013

   dx.doi.org/10.1021/ic4000457 | *Inorg. Chem.* 2013, 52, 5167−5175

Scheme 1. Synthetic Route for $PtAg_2$ Complexes

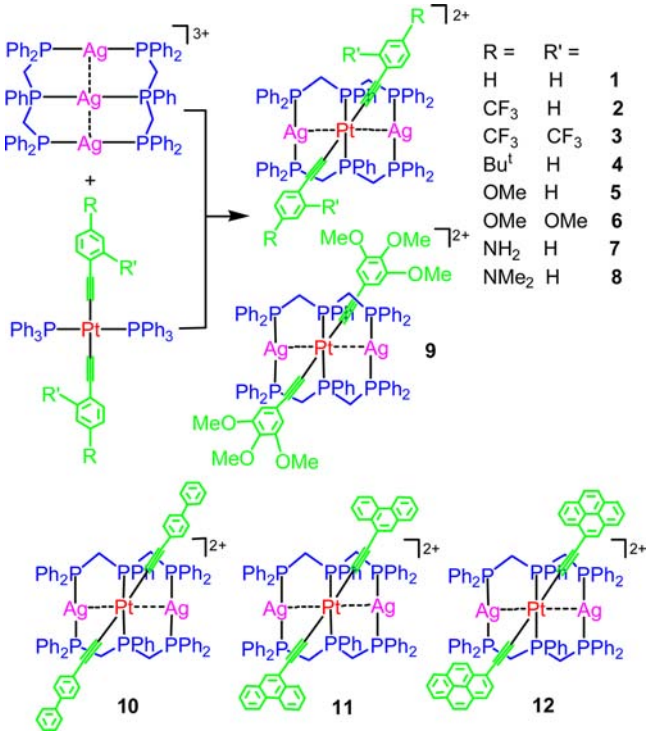

prepared in 79−86% yields. To modulate the spectroscopic and phosphorescent properties by changing the π-conjugated system, $PtAg_2$ complexes (**10**−**12**) with a progressively extended π-system in the aromatic acetylides were also prepared.

Ten structures of $PtAg_2$ complexes were determined by X-ray crystallography, including **1**·$2CH_2Cl_2$, **2**·CH_2Cl_2, **4**·$4CH_2Cl_2$, **4**(MeCN)·MeCN, **5**·$2CH_2Cl_2$·$2H_2O$, **5**$(py)_2$·2py, **9**·2acetone, **9**$(DMF)_2$·2DMF, **9**$(MeCN)_2$·$2Et_2O$, and **9**$(py)_2$·2py. Selected atomic distances and bond angles are provided in the Supporting Information (Tables S3 and S4). The structures depicted in Figure 1 reveal unambiguously that $PtAg_2$ centers are doubly linked by dpmp, which are highly stabilized by substantial Pt−Ag contact as well as four five-membered chelating rings. *trans*-$Pt(C{\equiv}CR)_2$ unit is located at the middle and two Ag(I) centers are at two sides.

The Ag−Pt−Ag angle is always 180° except for **2**·CH_2Cl_2 (171.988(16)°, Figure S1) with one of the two silver(I) centers bound to one perchlorate and **9**$(DMF)_2$·2DMF (151.735(15)°) with two Ag−DMF bonds (Figure 1d). Quite short Pt···Ag (2.9−3.1 Å) distances suggest the presence of significant Pt−Ag interaction.[3,9,10] The Pt···Ag distances are comparable to those found in doubly $Ph_2PCH_2PPh_2$ or Ph_2PNPPh_2 linked Pt^{II}−Ag^{I} complexes.[10] For **2**·CH_2Cl_2 (Figure S1), the distance of Pt1···Ag2 (3.0221(6) Å) with Ag2 bound to one O atom of perchlorate is obviously longer than that of Pt1···Ag1 (2.9469(6) Å) without Ag1−O linkage. The Pt···Ag distances in **9**$(MeCN)_2$·$2Et_2O$ (3.0774(7) Å, Figure 1b), **9**$(py)_2$·2py (3.0323(5) Å, Figure 1c), and **9**$(DMF)_2$·2DMF (3.0455(7) and 3.0472(8) Å, Figure 1d) with Ag−solvent bonds are obviously longer than that in **9**·2acetone (2.9782(10) Å, Figure 1a) without Ag−solvent bonds. Compared with the Pt···Ag distance in **4**·$4CH_2Cl_2$ (2.9555(5) Å, Figure S2a), those in **4**(MeCN)·MeCN (3.0258(4) and 3.0409(5) Å, Figure S2b) also become longer

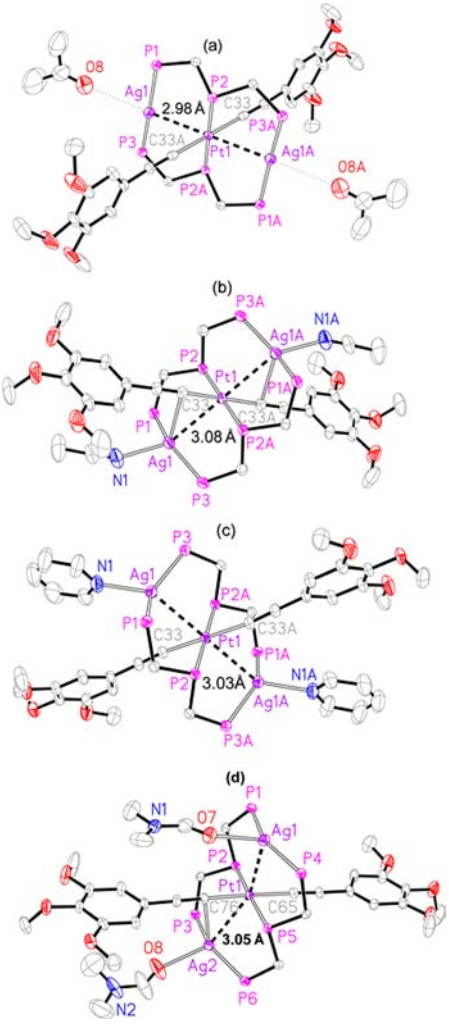

Figure 1. Perspective views (30% thermal ellipsoids) of cationic $PtAg_2$ complexes in **9**·2acetone (a), **9**$(MeCN)_2$·$2Et_2O$ (b), **9**$(py)_2$·2py (c), and **9**$(DMF)_2$·2DMF (d), showing obviously elongated Ag···Pt distance upon the formation of Ag−solvent bonds. Phenyl rings on the phosphorus atoms are omitted for clarity.

due to the formation of Ag−NCMe bonds. Similarly, the Pt···Ag distance in pyridine-bound complex **5**$(py)_2$·2py (3.0077(5) Å) is obviously longer than that in **5**·$2CH_2Cl_2$·$2H_2O$ (2.9318(10) Å). Accordingly, the formation of Ag−$OClO_3$ or Ag−solvent bonds results in much longer Pt···Ag distances.

The platinum(II) center is located at square-planar environment with trans-arranged P_2C_2 donors. The silver(I) center exhibits linear (Figure 1a), T-shaped or trigonal-planar geometry (Figures S1 and S2a) in the absence of the Ag−solvent bond. Upon the formation of Ag−solvent bonds, the silver(I) center exhibits a distorted T-shaped or trigonal-planar environment (Figure 1c) in the absence of Ag−acetylide bonds, whereas a tetrahedral geometry (Figure 1b) in the presence of Ag−acetylide bonds.

The variable-temperature ^{1}H NMR spectra of complex **9** (Figure S4) at 293−193 K suggest that the presence of fluxional structures in CD_2Cl_2 depending on the formation of the Ag−acetylide/perchlorate bond (Figure 1). Three singlets due to phenyl proton (H_a) with different intensity at 293 K (Figure S4) were distinctly changed in both chemical shift and relative intensity as the temperature was gradually lowered to 193 K.

dx.doi.org/10.1021/ic4000457 | *Inorg. Chem.* 2013, 52, 5167−5175

Similarly, three singlets for H_b (OCH_3 at two sides) or two singlets for H_c (OCH_3 at the middle) were also variable in both chemical shift and relative intensity when the temperature was lowered to 193 K. The presence of two or three signals for each equivalent proton together with temperature-dependent chemical shift and relative intensity revealed unambiguously three or more fluxional structures (Figure S4) depending on whether or not the formation of Ag−acetylide or Ag−$OClO_3$ bonds, as demonstrated unambiguously by X-ray crystallography. The relative percentages of various fluxional structures are alterable depending on the temperature and the solvents. The ^{31}P NMR spectra (Figure S5) are characteristic of Pt−P, Ag−P and P−P couplings with J_{Pt-P} = 2200−2600 Hz, J_{Ag-P} = 400−600 Hz, and J_{P-P} = 30−50 Hz. The ratio of integral area between Pt− and Ag−bound P atoms is 1: 2, coinciding well with their solid structures.

Computational Studies. Time-dependent DFT (TD-DFT) studies were performed on complex **1** (Tables S5). As depicted in Figure 2, the HOMO is mostly resident on

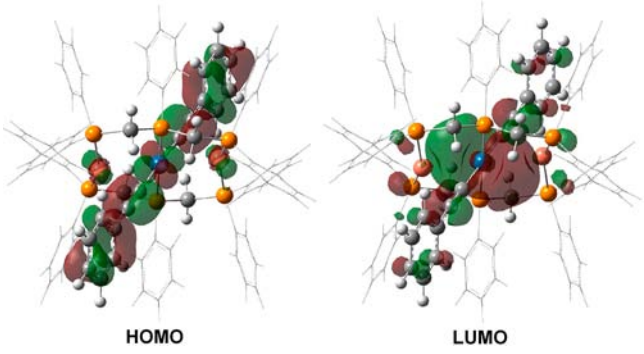

Figure 2. Spatial plots of the HOMO and LUMO of complex **1**.

phenylacetylide (66.9%) and $PtAg_2$ atoms (27.5%, 5d(Pt) and 4d(Ag)). The LUMO is uniformly distributed on dpmp (43.2%), $PtAg_2$ (34.0%, 6p(Pt) and 5p(Ag)) and phenylacetylide (22.8%). Electronic transitions due to HOMO → LUMO are thus ascribed to significant [π(C≡CR) → π^*(dpmp)] LLCT (ligand-to-ligand charge transfer) and $PtAg_2$ cluster centered [d → p] states with moderate [π → π^*(C≡CR)] IL (intraligand) character.

UV−vis Spectroscopic Properties. The UV−vis absorption spectra (Table 1) exhibit intense UV absorption bands at <300 nm and medium energy bands at 320−380 nm, originating mainly from ligand-centered transitions mixed with some metal-perturbed character. The broad low-energy bands at >380 nm are ascribed to significant [π(C≡CR) → π^*(dpmp)] LLCT and $PtAg_2$ cluster based [d → p] states together with moderate [π → π^*(C≡CR)] IL character as supported by TD-DFT studies. Solvent-dependent UV−vis spectra (Figure S6) indicate that the low-energy absorption bands show progressive blue-shift with the increase of solvent polarity, following toluene → CH_2Cl_2 → ethyl acetate → THF → acetone → MeOH → MeCN → DMF → pyridine. This is mostly ascribable to negative solvatochromism which is typical of charge transfer transitions involving the LLCT state.[9,10] The formation of solvent−metal bonds is likely another factor responsible for such a spectral blue-shift in coordination solvents such as MeCN, DMF, and pyridine.

As shown in Figure 3, relative to the low-energy band of **1** (R = R′ = H) at 402 nm, those of **2** (397 nm) and **3** (382 nm) are

Table 1. The UV-Vis Absorption Spectral Data of $PtAg_2$ Complexes 1−12 in CH_2Cl_2 Solutions

complex	λ_{abs}/nm (ε/dm^3 mol^{-1} cm^{-1})
1	231 (82280), 270 (42570), 349 (29130), 402 (13470)
2	231 (88670), 269 (47490), 355 (32480), 397 (11520)
3	230 (83990), 269 (38150), 303 (24350), 345 (31920), 358 (31770), 382 (13300)
4	230 (79100), 269 (45260), 347 (26330), 411 (15210)
5	230 (78720), 268 (43350), 342 (24370), 423 (14230)
6	230 (95150), 268 (46550), 313 (24640), 345 (28460), 438 (17150)
7	229 (75240), 270 (40870), 342 (26500), 448 (14790)
8	230 (75440), 269 (37420), 339 (32040), 479 (15950)
9	230 (103000), 269 (43700), 383 (50000), 444 (14300)
10	230 (89100), 294 (56800), 345 (27200), 410 (16930)
11	229 (93700), 278 (35500), 290 (40000), 360 (35100), 379 (37400), 420 (20600)
12	229 (103000), 278 (42300), 289 (47100), 357 (52200), 376 (53800), 445 (16000)

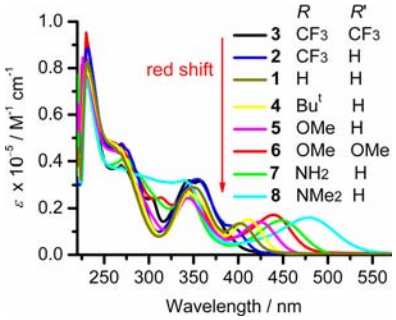

Figure 3. The UV−vis absorption spectra of $PtAg_2$ complexes in CH_2Cl_2 at ambient temperature, showing a progressive red-shift of the low-energy bands with the increased electron-donating character of *R* and *R*′ in phenylacetylide.

gradually blue-shifted because introducing one or two electron-withdrawing CF_3 to phenylacetylide would lower the HOMO (mainly π orbital of phenylacetylide) level and thus increase the HOMO−LUMO gap of LLCT and IL states. In contrast, the low-energy absorption bands of **4** (411 nm), **5** (423 nm), **6** (438 nm), **7** (448 nm), and **8** (479 nm) with one or two Bu^t, OMe, NH_2, or NMe_2 exhibit progressive red-shift compared with **1** (402 nm) since introduction of electron-donating substituents to phenylacetylide would raise the HOMO level and thus reduce HOMO−LUMO gap of LLCT and IL states. Thus, the spectral shift trend due to the electronic effects of R or R′ coincides perfectly with the assignment that the low-energy absorption bands display significant character of LLCT and IL states.

Increasing π-conjugated system in the aromatic acetylide is another feasible approach to induce red-shift of the low-energy absorption bands. As depicted in Figure 4, the low-energy absorption bands of $PtAg_2$ complexes show stepwise red-shifts, following 402 nm (**1**) → 410 nm (**10**) → 420 nm (**11**) → 445 nm (**12**). Since the HOMO (π orbital of aromatic acetylide) level is increasingly raised with the extension of π-conjugated system in aromatic acetylide, the HOMO−LUMO gap is progressively reduced.

Phosphorescent Properties. Upon irradiation at λ_{ex} > 300 nm, complexes **1**−**12** (Table 2) exhibit bright or brilliant luminescence in both fluid CH_2Cl_2 solutions and solid states at ambient temperature. Large Stokes shifts together with a

dx.doi.org/10.1021/ic4000457 | Inorg. Chem. 2013, 52, 5167−5175

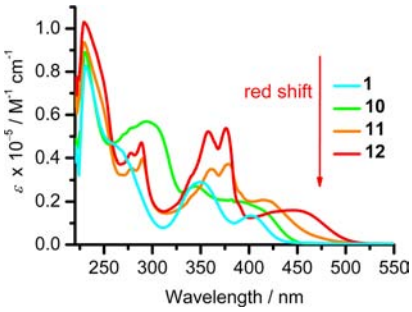

Figure 4. The UV−vis absorption spectra of $PtAg_2$ complexes in CH_2Cl_2 solutions at ambient temperature, showing a progressive red-shift of the low-energy bands with an increased π-conjugated system in aromatic acetylides.

Table 2. Luminescence Data of $PtAg_2$ Complexes in Fluid CH_2Cl_2 and Solid State at Ambient Temperature

	CH_2Cl_2			solid		
	λ_{em}/nm	τ_{em}/μs	Φ_{em}/%	λ_{em}/nm	τ_{em}/μs	Φ_{em}/%
1	490	0.08	1.0	500	1.32	27.3
2	476	0.014	3.4	491	1.48	44.4
3	463	0.37	9.3	467	5.80	9.7
4	502	0.13	3.5	504	1.47	74.1
5	524	1.46	14.3	520	2.09	28.6
6	552	4.72	22.5	548	2.63	40.2
7	604	0.04	weak	593	1.84	24.0
8	625	0.78	1.0	618	1.01	2.8
9	543	5.15	14.3	555	4.98	39.2
10	504	4.33	20.5	529	4.32	5.2
11	563	16.30	13.4	558	16.34	1.6
12	661	35.90	1.2	658	1.03	weak

microsecond or sub-microsecond range of lifetimes imply that the luminescence is phosphorescent in nature with triplet excited states. The emission spectra (Figure S7) are solvent-dependent to afford 7−19 nm (270−715 cm^{-1}) blue-shifts in coordination solvents such as pyridine, DMF, MeCN, etc. due to the formation of Ag−solvent bonds. The emission intensity is enhanced with the increase of the concentrations at $<10^{-4}$ M, but self-quenching occurs in higher concentrations.

These $PtAg_2$ complexes display moderate phosphorescent quantum yields in fluid CH_2Cl_2 solutions (Φ_{em} = 1.0−22.5%) whereas much higher quantum yields in solid states (Φ_{em} = 1.6−74.1%) at ambient temperature. As demonstrated by ^{1}H NMR spectral studies, fluxional structures are existent for $PtAg_2$ complexes in fluid CD_2Cl_2 solutions, originating from unsaturated coordination character on silver(I) centers which tend to bind further to acetylide C or perchlorate O atoms. Nevertheless, such Ag−C and Ag−O bonds are quite labile, so that rapid formation/disruption of metastable coordination bonds would become an effective nonradiative decay pathway, thus deactivating the triplet excited states and reducing significantly the phosphorescence efficiency in fluid solutions. It is noteworthy that the phosphorescence in $PtAg_2$ complexes with $C{\equiv}CC_6H_4NH_2$-4 or $C{\equiv}CC_6H_4NMe_2$-4 is quite weak due to the strong electron-donating character of -NH_2 or -NMe_2, which favors intramolecular electron transfer so as to quench significantly the emissive triplet state.

As shown in Figure 5, the phosphorescence in a series of $PtAg_2$ complexes was perfectly modulated by modifying the substituent in aromatic acetylide. The emission maxima follow

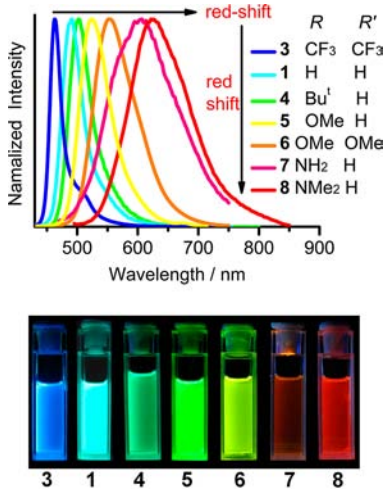

Figure 5. The emission spectra and photographic images (irradiation at 365 nm) of a series of $PtAg_2$ complexes (2.0×10^{-5} M) in fluid CH_2Cl_2 solutions, showing progressive red-shifted emission bands and luminescence colors with an increased electron-donating capability of R and R′ substituents in the phenylacetylides.

463 nm (**3**) → 476 nm (**2**) → 490 nm (**1**) → 502 nm (**4**) → 524 nm (**5**) → 552 nm (**6**) → 604 nm (**7**) → 625 nm (**8**), in which the phosphorescence color shows a progressive red-shift in the order of deep blue (**3**) → blue (**2**) → cyan (**1**) → green (**4**) → yellow-green (**5**) → yellow (**6**) → orange (**7**) → red (**8**). It is obvious that the emission spectra are progressively red-shifted with the gradually increased electron-donating capability of R and R′ in $C{\equiv}CC_6H_3(R',R)$-2,4 following CF_3 → H → Bu^t → OMe → NH_2 → NMe_2, ascribed to the increasingly raised energy level of the HOMO (mainly π orbital of acetylide) and thus gradually reduced HOMO−LUMO gap. Such a spectral shift coincides perfectly with the assignment that the phosphorescence originates primarily from $^3[\pi(C{\equiv}CR) \rightarrow \pi^*(dpmp)]$ ^{3}LLCT and $^3[\pi \rightarrow \pi^*(C{\equiv}CR)]$ ^{3}IL triplet excited states with significant $PtAg_2$ cluster centered $^3[d \rightarrow p]$ character that is modified by substantial Pt−Ag contact depending on the Pt···Ag distance.

The solution phosphorescence of $PtAg_2$ complexes was also modulated by introducing a more extended π-system in aromatic acetylides. As depicted in Figure 6, the phosphorescence shows a progressive red-shift following 490 nm (**1**) → 504 nm (**10**) → 563 nm (**11**) → 661 (**12**) with cyan, green, yellow, and red light emitting, respectively. This is readily understandable because progressive increase of π-conjugated system in aromatic acetylide would raise the π orbital level (HOMO) and accordingly reduce the HOMO−LUMO gap of ^{3}LLCT/^{3}IL triplet excited states. With the progressive increase of a π-conjugated system in aromatic acetylide ligands, the phosphorescent lifetimes of $PtAg_2$ complexes exhibit a gradual increase following 0.08 μs (**1**) → 4.33 μs (**10**) → 16.30 μs (**11**) → 35.90 (**12**) in fluid CH_2Cl_2, ascribable likely to the gradually enhanced IL character in aromatic acetylide ligands and the progressively reduced [d → p] character in $PtAu_2$ cluster.

Vapor-Responsive Phosphorescence Changes. Interestingly, the phosphorescence in the solid state is mostly sensitive to vapor of MeCN, DMF, pyridine, etc. with coordination character. When powder, crystals, or films (Figures 7 and 8, Figure S8) of these $PtAg_2$ complexes are exposed to vapor of MeCN, pyridine, or DMF, remarkable emitting color changes occur within dozens of seconds to a few

dx.doi.org/10.1021/ic4000457 | Inorg. Chem. 2013, 52, 5167−5175

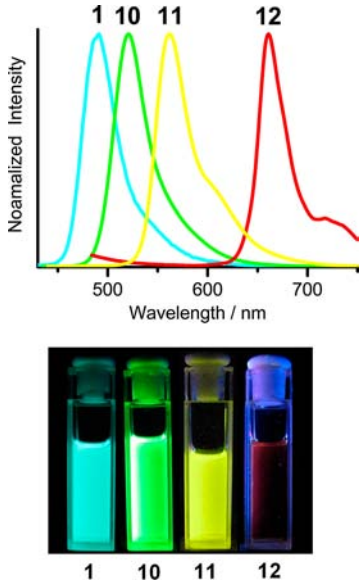

Figure 6. The emission spectra and photographic images of $PtAg_2$ complexes **1** and **10**–**12** in fluid CH_2Cl_2 (2.0×10^{-5} M), showing a progressive red-shift of the low-energy bands with increased π-conjugated system in aromatic acetylide.

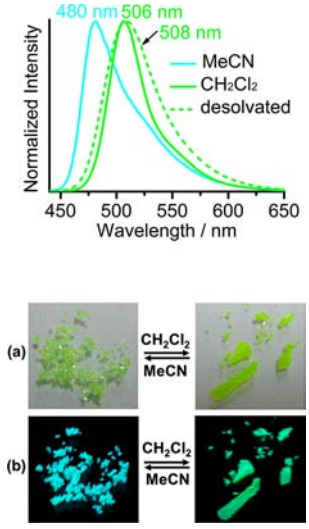

Figure 7. Emission spectra (top) and photographic images (bottom) of the crystals of **4**(MeCN)·MeCN and **4**·$4CH_2Cl_2$ under ambient light (a) and UV (365 nm) light (b), showing reversible interconversion between crystals **4**(MeCN)·MeCN and **4**·$4CH_2Cl_2$ upon exposing to CH_2Cl_2 or MeCN vapor.

minutes depending on the crystallinity of the solids or thickness of the films, in which the emission bands show obvious blue-shifts.

As depicted in Figure 7, the crystals of **4**·$4CH_2Cl_2$ display reversible phosphorescence vapochromism in response to vapor of MeCN with the emission at 506 nm being blue-shifted to 480 nm. Upon exposure to MeCN vapor, green phosphorescence in the crystals of **4**·$4CH_2Cl_2$ turned to blue emitting due to formation of **4**(MeCN)·MeCN containing both coordinated and crystallized MeCN. Conversely, upon exposure to CH_2Cl_2 vapor, blue emitting crystals of **4**(MeCN)·MeCN reverted to green phosphorescent **4**·$4CH_2Cl_2$ in a few minutes. Since the Pt···Ag distance in **4**(MeCN)·MeCN (3.0258(4) Å) is obviously longer than that

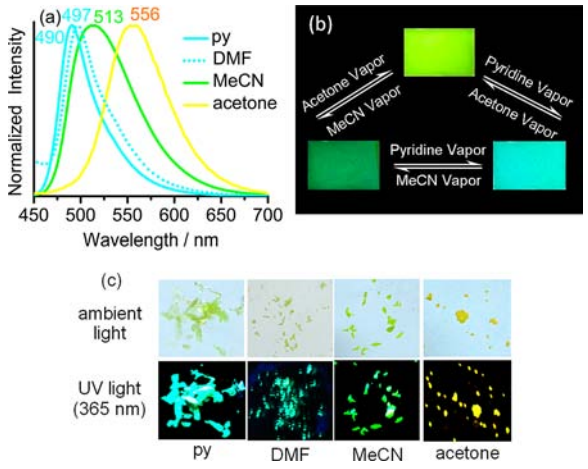

Figure 8. The emission spectra (a) and photographic images of PMMA films (b) of **9** and the crystals (c) of **9**$(py)_2$·2py, **9**$(DMF)_2$·2DMF, **9**$(MeCN)_2$·$2Et_2O$, and **9**·2acetone under ambient and UV (365 nm) light irradiation.

in **4**·$4CH_2Cl_2$ (2.9555 Å), MeCN vapor triggered blue-shift of the emission is mostly relevant to the formation of MeCN–Ag bonds and the reduced Pt–Ag interaction in **4**(MeCN)·MeCN which would increase the HOMO–LUMO gap and thus the emissive energy.

Upon exposure to pyridine vapor, the crystals of **5**·$2CH_2Cl_2$·$2H_2O$ (Figure S8) converted to **5**$(py)_2$·2py with both coordinated and solvated pyridine, in which green emission at 520 nm turned to cyan luminescence at 490 nm in a few minutes. Conversely, cyan-emitting crystals of **5**$(py)_2$·2py reverted reversibly to green-emitting **5**·$2CH_2Cl_2$·$2H_2O$ upon exposure to CH_2Cl_2 vapor. TD-DFT calculations were conducted on **5**·$2CH_2Cl_2$·$2H_2O$ (Table S6) and **5**$(py)_2$·2py (Table S7) using crystallographic parameters. The HOMO–LUMO gap (Figure S11) in **5**$(py)_2$·2py (3.86 eV) is obviously larger than that in **5**·$2CH_2Cl_2$·$2H_2O$ (3.45 eV) as a consequence of the formation of Ag–pyridine coordination bonds for the former. The calculated triplet state transition energy in **5**$(py)_2$·2py (2.77 eV, Table S7) is obviously higher than that in **5**·$2CH_2Cl_2$·$2H_2O$ (2.49 eV, Table S6). Mayer bond order calculation suggests that the Pt–Ag bond order in **5**$(py)_2$·2py (0.24) is distinctly smaller than that in **5**·$2CH_2Cl_2$·$2H_2O$ (0.27). This is well correlated with a weaker Pt–Ag interaction in **5**$(py)_2$·2py (d_{Pt-Ag} = 3.0077(5) Å) due to a longer Pt···Ag distance than that in **5**·$2CH_2Cl_2$·$2H_2O$ (d_{Pt-Ag} = 2.9318(10) Å). Thus, the emission blue-shift of **5**·$2CH_2Cl_2$·$2H_2O$ (520 nm) upon conversion to **5**$(py)_2$·2py (490 nm) is ascribable to the formation of Ag–pyridine bonds and consequently the reduced Pt–Ag interaction, which perturbs the metal centers and increases the transition energy.

When complex **9** was crystallized in acetone, MeCN, DMF, and pyridine, the isolated crystals of **9**·2acetone, **9**$(MeCN)_2$·$2Et_2O$, **9**$(DMF)_2$·2DMF and **9**$(py)_2$·2py exhibit brilliant yellow, green, cyan, and cyan luminescence (Figure 8) with the emission maxima at 556, 513, 497, and 490 nm, respectively. Relative to **9**·2acetone (556 nm) with solvate acetone, a significant blue-shift of the emission in **9**$(MeCN)_2$·$2Et_2O$ (513 nm), **9**$(DMF)_2$·2DMF (497 nm), or **9**$(py)_2$·2py (490 nm) is ascribable to the bonding of MeCN, DMF, or pyridine to silver(I) centers (Figure 1), in which the Pt···Ag distances in **9**$(MeCN)_2$·$2Et_2O$ (3.08 Å), **9**$(DMF)_2$·2DMF (3.05 Å), or **9**$(py)_2$·2py (3.03 Å) are

dx.doi.org/10.1021/ic4000457 | Inorg. Chem. 2013, 52, 5167–5175

obviously longer than that in **9**·2acetone (2.98 Å). Solvent coordination induces distinct elongation in Pt···Ag distances, and thus the reduction of Pt−Ag interaction may be the key factor for blue-shift of the emission.

Dynamic emission spectral changes (Figure 9) were recorded upon exposing the crystals of **9**·2acetone to pyridine vapor, in

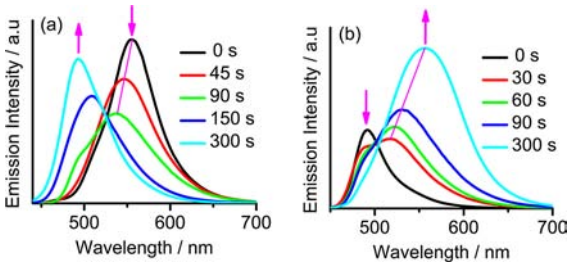

Figure 9. Dynamic emission spectral changes upon exposure of the crystals of (a) **9**·2acetone to pyridine vapor, and (b) **9**$(py)_2$·2py to acetone vapor.

which the emission at 556 nm is gradually blue-shifted to 490 nm within 5 min due to the formation of **9**$(py)_2$·2py. Conversely, exposing the crystals of **9**$(py)_2$·2py to acetone vapor induces progressive red-shift of the emission at 490−556 nm upon the conversion to **9**·2acetone. The X-ray diffraction (XRD) patterns recorded in a vapochromic cycle of **9**·2acetone ⇆ **9**$(py)_2$·2py are depicted in Figure 10, showing unambigu-

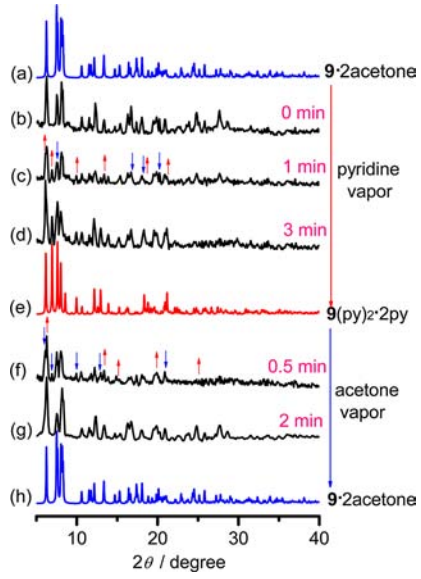

Figure 10. The XRD spectra recorded in a reversible vapochromic cycle of **9**$(py)_2$·2py ⇆ **9**·2acetone, showing variations of the PXRD patterns from (c−d) in the process **9**·2acetone → **9**$(py)_2$·2py, and those from (f−g) in the reversed process **9**$(py)_2$·2py → **9**·2acetone. (a)/(h): The simulated pattern of **9**·2acetone. (b) The measured pattern of **9**·2acetone. (e) The simulated pattern of **9**$(py)_2$·2py.

ously the interconversion between crystalline **9**$(py)_2$·2py and **9**·2acetone through vapor sorption within a few minutes. Thus, the vapor-triggered solid-state phosphorescence changes are totally reversible.

Luminescence vapochromism has been found in some d^6, d^8, and d^{10} metal complexes, arising mostly from vapor-triggered variations in intramolecular or intermolclecular interactions including metal−solvent bonds, metallophilic contacts, π−π stacking, hydrogen bonding, host−guest affinity, reversible isomerization, etc.[27,28] A series of d^{10}-d^{10} complexes with Au−Tl, Au−Ag, and Au−Cu heterometallic arrays[29,30] have been demonstrated to exhibit remarkable luminescence changes in response to vapors of coordination solvents due to reversible formation/disruption of Tl/Ag/Cu−solvent bonds, thus affecting the emissive states relevant to d^{10}-d^{10} metallophilic interaction. The $PtAg_2$ complexes with significant phosphorescence vapochromism represent the first family of vapor-responsive solid materials based on d^8-d^{10} heteronuclear complexes for detection of volatile organic compounds (VOCs) with coordination character, resulting from perturbation of d^8-d^{10} metallophilic interaction in the excited states due to the formation/disruption of Ag−solvent bonds.

CONCLUSIONS

Highly phosphorescent d^8-d^{10} $PtAg_2$ alkynyl complexes are elaborately designed. The solution phosphorescence was systematically modulated by modifying substituents as well as π-conjugated systems in aromatic acetylide so as to achieve bright phosphorescence with various emitting colors. The solid-state phosphorescence is successfully modulated by external stimulus. Crystals, powders, or films of these $PtAg_2$ complexes exhibit reversible stimuli-responsive phosphorescence switch upon exposure to vapor of MeCN, pyridine, or DMF due to the formation of solvent−Ag bonds, which elongates Pt···M distances and accordingly reduces Pt−Ag interaction, thus resulting in an obvious blue shift of the phosphorescence emission. As demonstrated experimentally and theoretically, the phosphorescence emission arises from significant [π(C≡CR) → π*(dpmp)] LLCT and $PtAg_2$ cluster-based [d → p] transitions that are modified by substantial Pt−Ag interaction depending on the Pt···Ag distances, together with moderate [π → π*(C≡CR)] IL character.

EXPERIMENTAL SECTION

General Procedures and Materials. All manipulations were conducted under a dry argon atmosphere using Schlenk techniques and vacuum-line systems unless otherwise specified. The solvents were dried, distilled, and degassed prior to use except that those for spectroscopic measurements were of spectroscopic grade. Bis(diphenylphosphinomethyl)phenylphosphine (dpmp) was prepared by a synthetic procedure described in the literature.[31] Other reagents were purchased from commercial sources and used as received unless stated otherwise. The precursor complexes $Pt(PPh_3)_2(C{\equiv}CR)_2$ were prepared by reactions of $Pt(PPh_3)_2Cl_2$ (0.5 mmol), alkynyl ligands (1.1 mmol), CuI (1 mg), and NEt_3 (1 mL) in chloroform (50 mL) with stirring at 50 °C for 5 h. The products were purified by chromatography on silica gel columns using CH_2Cl_2- petroleum ether as eluent.

$[PtAg_2(dpmp)_2(C{\equiv}CC_6H_5)_2](ClO_4)_2$ (1). To a CH_2Cl_2 (20 mL) solution of dpmp (50.6 mg, 0.1 mmol) was added $Ag(tht)(ClO_4)$ (29.5 mg, 0.1 mmol) with stirring for 30 min. Upon the addition of $Pt(PPh_3)_2(C{\equiv}CC_6H_5)_2$ (46.1 mg, 0.05 mmol), the solution became pale yellow with stirring at ambient temperature for 4 h. The solution was concentrated to 2 mL, which was chromatographed on a silica gel column using CH_2Cl_2-MeCN (8:1) as eluent to afford the product as a pale yellow solid. Yield: 85%. Anal. Calcd for $C_{80}H_{68}Ag_2Cl_2O_8P_6Pt$: C, 52.65; H, 3.76. Found: C, 52.68; H, 3.86. ESI-MS *m*/*z* (%): 1725.4 (100) $[M-ClO_4]^+$, 814.3 (10) $[M-2ClO_4]^{2+}$. IR (KBr) ν/cm^{-1}: 2096w (C≡C), 1103s (ClO_4). ^{1}H NMR (CD_2Cl_2) δ/ppm: 7.96−7.89 (m, 6H), 7.77−7.65 (m, 6H), 7.54−7.35 (m, 22H), 7.28−7.16 (m, 8H), 7.15−7.06 (m, 6H), 7.03−6.94 (m, 6H), 6.74−6.70 (m, 2H), 6.65−6.63 (m, 1H), 6.40−6.37 (m, 2H), 6.36−6.34 (m, 1H), 5.04−4.84 and 4.53−4.41 (m,4H), 4.14−4.06 and 3.97−3.88 (m, 4H). ^{31}P

dx.doi.org/10.1021/ic4000457 | *Inorg. Chem.* 2013, 52, 5167−5175

NMR (CD_2Cl_2) δ/ppm: 11.5 (m, 1P, J_{Pt-P} = 2432 Hz, J_{P-P} = 34.6 Hz), 3.9 (m, 2P, J_{Ag-P} = 527 Hz, J_{P-P} = 37.2 Hz).

Instead, it was also prepared by the following synthetic procedure. To a CH_2Cl_2 (20 mL) solution of $[Ag_3(dpmp)_2](ClO_4)_3$ (107.1 mg, 0.05 mmol) was added $Pt(PPh_3)_2(C{\equiv}CPh)_2$ (46.1 mg, 0.05 mmol). The solution changed to pale yellow upon stirring at ambient temperature for 4 h. Upon the solution being concentrated to 2 mL, it was chromatographed onto a silica gel column. The first colorless band was eluted using CH_2Cl_2-MeCN (10: 1), which was identified as $Ag(PPh_3)_4(ClO_4)$ (20 mg). The second band was eluted using CH_2Cl_2-MeCN (8:1) to give the product as a yellow solid. Yield: 80%.

$[PtAg_2(dpmp)_2(C{\equiv}CC_6H_4CF_3\text{-}4)_2](ClO_4)_2$ (2). This compound was prepared by the same synthetic procedure as that of **1** except for using 1-ethynyl-4-trifluoromethylbenzene instead of phenylacetylene. Yield: 79%. Anal. Calcd for $C_{82}H_{66}Ag_2Cl_2F_6O_8P_6Pt$: C, 50.23; H, 3.39. Found: C, 50.24; H, 3.48. ESI-MS m/z (%): 1861.6 (100) $[M-ClO_4]^+$. IR (KBr) ν/cm^{-1}: 2099w (C≡C), 1102s (ClO_4). ^{1}H NMR (CD_2Cl_2) δ/ppm: 7.94−7.87 (m, 6H), 7.75−7.64 (m, 6H), 7.50−7.31 (m, 22H), 7.27−6.93 (m, 18H), 6.74−6.70 (t, 2H, J = 7.7 Hz), 6.64−6.62 (d, 1H, J = 8.3 Hz), 6.35−6.31 (m, 3H), 4.99−4.90 and 4.54−4.46 (m, 4H), 4.16−4.07 and 3.97−3.89 (m, 4H). ^{31}P NMR (CD_2Cl_2) δ/ppm: 11.8 and 11.0 (m, 1P, J_{Pt-P} = 2392 Hz, J_{P-P} = 34.1 Hz), 4.7 and 3.8 (m, 2P, J_{Ag-P} = 527 Hz, J_{P-P} = 36.5 Hz).

$[PtAg_2(dpmp)_2(C{\equiv}CC_6H_3(CF_3)_2\text{-}2,4)_2](ClO_4)_2$ (3). This compound was prepared by the same synthetic procedure as that of **1** except for using 1-ethynyl-2,4-bis-trifluoromethylbenzene instead of phenylacetylene. Yield: 82%. Anal. Calcd for $C_{84}H_{64}Ag_2Cl_2F_{12}O_8P_6Pt$: C, 48.11; H, 3.08. Found: C, 48.26; H, 3.05. ESI-MS m/z (%): 1997.0 (100) $[M-ClO_4]^+$, 1790.1 (30) $[M-AgClO_4-ClO_4]^+$, 948.4 (35) $[M-2ClO_4]^{2+}$. IR (KBr) ν/cm^{-1}: 2105w (C≡C), 1103s (ClO_4). ^{1}H NMR (CD_2Cl_2) δ/ppm: 8.07−8.02 (m, 6H), 7.98−7.93 (m, 1H), 7.86−7.82 (m, 3H), 7.78−7.23 (m, 2H), 7.62−7.28 (m, 34H), 7.21−6.13 (m, 4H), 7.01−6.95 (m, 3H), 6.89−6.85 (m, 3H), 4.74−4.68 and 4.46−4.50 (m, 4H), 4.40−4.35 and 3.99−3.94 (m, 4H). ^{31}P NMR (CD_2Cl_2) δ/ppm: 8.6 (m, 1P, J_{Pt-P} = 2384 Hz, J_{P-P} = 35.2 Hz), 7.8 (m, 2P, J_{Ag-P} = 509 Hz, J_{P-P} = 36.8 Hz).

$[PtAg_2(dpmp)_2(C{\equiv}CC_6H_4Bu^t\text{-}4)](ClO_4)_2$ (4). This compound was prepared by the same synthetic procedure as that of **1** except for using 1-ethynyl-4-butylbenzene instead of phenylacetylene. Yield: 82%. Anal. Calcd for $C_{88}H_{84}Ag_2Cl_2O_8P_6Pt{\cdot}3H_2O$: C, 53.08; H, 4.56. Found: C, 53.05; H, 4.65. ESI-MS m/z (%): 1837.9 (25) $[M-ClO_4]^+$, 869.0 (100) $[M-2ClO_4]^{2+}$. IR (KBr) ν/cm^{-1}: 2095w (C≡C), 1101s (ClO_4). ^{1}H NMR (CD_2Cl_2) δ/ppm: 7.94−7.87 (m, 6H), 7.75−7.63 (m, 6H), 7.51−7.31 (m, 25H), 7.26−7.15 (m, 7H), 7.08−7.04 (t, 5H, J = 7.5 Hz), 7.00−6.93 (m, 3H), 6.73−6.63(m, 3H),6.38−6.34 (m, 3H), 5.05−4.86 and 4.59−4.43 (m, 4H), 4.16−4.07 and 3.97−3.89 (m, 4H), 2.53, 2.49, and 2.48 (s, 18H). ^{31}P NMR (CD_2Cl_2) δ/ppm: 11.7 and 11.0 (m, 1P, J_{Pt-P} = 2442 Hz, J_{P-P} = 35.3 Hz), 4.6 (m, 2P, J_{Ag-P} = 527 Hz, J_{P-P} = 37.0 Hz).

$[PtAg_2(dpmp)_2(C{\equiv}CC_6H_4OMe\text{-}4)_2](ClO_4)_2$ (5). This compound was prepared by the same synthetic procedure as that of **1** except for using 1-ethynyl-4-methoxybenzene instead of phenylacetylene. Yield: 82%. Anal. Calcd for $C_{82}H_{72}Ag_2Cl_2O_{10}P_6Pt$: C, 52.25; H, 3.85. Found: C, 52.38; H, 3.90. ESI-MS m/z (%): 1785.5 (100) $[M-ClO_4]^+$. IR (KBr) ν/cm^{-1}: 2090w (C≡C), 1095s (ClO_4). ^{1}H NMR (CD_2Cl_2) δ/ppm: 7.92−7.85 (m, 6H), 7.73−7.62 (m, 6H), 7.49−7.31 (m, 22H), 7.25−7.13 (m, 7H), 7.07−7.03 (t, 4H, J = 7.5 Hz), 6.98−6.90 (m, 3H), 6.69−6.61(m, 3H),6.53−6.46 (m, 4H), 6.29−6.26 (m, 3H), 4.92−4.85 and 4.48−4.42 (m, 4H), 4.09−4.01 and 3.92−3.85 (m, 4H), 3.77 and 3.71 (s, 6H). ^{31}P NMR (CD_2Cl_2) δ/ppm: 11.8 and 10.9 (m, 1P, J_{Pt-P} = 2442 Hz, J_{P-P} = 35.3 Hz), 4.1 and 2.9 (m, 2P, J_{Ag-P} = 519 Hz, J_{P-P} = 36.9 Hz).

$[PtAg_2(dpmp)_2(C{\equiv}CC_6H_3(OMe)_2\text{-}2,4)_2](ClO_4)_2$ (6). This compound was prepared by the same synthetic procedure as that of **1** except for using 1-ethynyl-2,4-dimethoxybenzene instead of phenylacetylene. Yield: 82%. Anal. Calcd for $C_{84}H_{76}Ag_2Cl_2O_{12}P_6Pt{\cdot}3/2CH_2Cl_2$: C, 49.55; H, 3.84. Found: 49.92; H, 3.91. ESI-MS m/z (%): 1845.8 (100) $[M-ClO_4]^+$. IR (KBr) ν/cm^{-1}: 2097w (C≡C), 1098s (ClO_4). ^{1}H NMR (CD_2Cl_2) δ/ppm: 7.93−7.88 (m, 3H), 7.71−7.61 (m, 9H), 7.47−7.23 (m, 26H), 7.18−7.13 (m, 6H), 7.09−7.06 (t, 3H, J = 7.4 Hz), 6.99−6.91 (m, 3H), 6.64−6.60 (m, 2H),6.40−6.38 (d, 1H), 6.32−6.27 (m, 2H), 6.20−6.15 (m, 1H), 4.93−4.75 and 4.44−4.39 (m, 4H), 4.35−4.26 and 4.08−4.00 (m, 4H), 3.79, 3.77, 3.71, 3.70, 3.50, and 3.13 (s, 12H). ^{31}P NMR (CD_2Cl_2) δ/ppm: 12.9 and 11.6 (m, 1P, J_{Pt-P} = 2456 Hz, J_{P-P} = 34.4 Hz), 7.6 (m, 2P, J_{Ag-P} = 517 Hz, J_{P-P} = 36.7 Hz).

$[PtAg_2(dpmp)_2(C{\equiv}CC_6H_4NH_2\text{-}4)_2](ClO_4)_2$ (7). This compound was prepared by the same synthetic procedure as that of **1** except for using 1-ethynyl-4-aminobenzene instead of phenylacetylene. Yield: 82%. Anal. Calcd for $C_{80}H_{70}Ag_2Cl_2N_2O_8P_6Pt$: C, 51.80; H, 3.80; N, 1.51. Found: C, 51.74; H, 3.92; N, 1.45. ESI-MS m/z (%): 1755.3 (100) $[M-ClO_4]^+$, 828.5 (5) $[M-2ClO_4]^{2+}$. IR (KBr) ν/cm^{-1}: 2090w (C≡C), 1102s (ClO_4). ^{1}H NMR (CD_2Cl_2) δ/ppm: 7.88−7.83 (m, 6H), 7.69−7.65 (m, 4H), 7.62−7.56 (m, 2H), 7.49−7.31 (m, 22H), 7.24−7.13 (m, 8H), 7.05−7.02 (t, 4H, J = 7.5 Hz), 6.96−6.89 (m, 3H), 6.67−6.63 (m, 2H), 6.40−6.36 (m, 1H), 6.28−6.22 (m, 3H), 6.19−6.15 (m, 3H), 4.89−4.70 and 4.44−4.27 (m, 4H),4.05−3.96 and 3.88−3.76 (m, 8H). ^{31}P NMR (CD_2Cl_2) δ/ppm: 11.7 (m, 1P, J_{Pt-P} = 2446 Hz, J_{P-P} = 36.8 Hz), 3.6 (m, 2P, J_{Ag-P} = 521 Hz, J_{P-P} = 36.5 Hz).

$[PtAg_2(dpmp)_2(C{\equiv}CC_6H_4NMe_2\text{-}4)_2](ClO_4)_2$ (8). This compound was prepared by the same synthetic procedure as that of **1** except for using 1-ethynyl-4-dimethylaminobenzene instead of phenylacetylene. Yield: 81%. Anal. Calcd for: $C_{84}H_{78}Ag_2Cl_2N_2O_8P_6Pt{\cdot}2CH_2Cl_2$: C, 49.64; H, 3.97; N, 1.35. Found: C, 49.78; H, 4.04; N, 1.30. ESI-MS m/z (%): 1811.3 (100) $[M-ClO_4]^+$. IR (KBr) ν/cm^{-1}: 2090w (C≡C), 1097s (ClO_4). ^{1}H NMR (CD_2Cl_2) δ/ppm: 7.87−7.82 (m, 6H), 7.69−7.64 (m, 4H), 7.62−7.57 (m, 2H), 7.48−7.31 (m, 22H), 7.24−7.12 (m, 8H), 7.06−7.04 (t, 4H, J = 7.4 Hz), 6.96−6.90 (m, 4H), 6.67−6.63 (m, 2H),6.49−6.41 (m, 2H), 6.31−6.30 (d, 4H, J = 5.0 Hz), 4.88−4.70 and 4.44−4.27 (m, 4H), 4.07−3.99 and 3.90−3.81 (m, 4H), 2.94, 2.90, and 2.89 (s, 12H). ^{31}P NMR (CD_2Cl_2) δ/ppm: 11.6 (m, 1P, J_{Pt-P} = 2432 Hz, J_{P-P} = 34.2 Hz), 4.0 and 3.2 (m, 2P, J_{Ag-P} = 518 Hz, J_{P-P} = 34.7 Hz).

$[PtAg_2(dpmp)_2(C{\equiv}CC_6H_2(OMe)_3\text{-}3,4,5)_2](ClO_4)_2$ (9). This compound was prepared by the same synthetic procedure as that of **1** except for the use of 5-ethynyl-1,2,3-trimethoxybenzene instead of phenylacetylene. Yield: 86%. Anal. Calcd for $C_{86}H_{80}Ag_2Cl_2O_{14}P_6Pt$: C, 51.51; H, 4.02. Found: C, 51.56; H, 3.99. ESI-MS m/z (%): 1905.6 (100) $[M-ClO_4]^+$. IR (KBr) ν/cm^{-1}: 2092w (C≡C), 1099s (ClO_4). ^{1}H NMR (CD_2Cl_2) δ/ppm: 7.89−7.81 (m, 6H), 7.75−7.70 (m, 3H), 7.63−7.58 (m, 3H), 7.48−7.34 (m, 20H), 7.31−7.27 (t, 1H, J = 7.4 Hz), 7.23−7.19 (t, 3H, J = 7.5 Hz), 7.15−7.10(m, 3H), 7.09−7.01 (m, 6H), 6.94−6.85(m, 3H), 6.68−6.64 (m, 2H), 5.79, 5.76, and 5.65 (s, 4H), 5.06−4.87, 4.68−4.51 (m, 4H), 4.14−4.05, 3.93−3.84 (m, 4H), 3.67, 3.64, 3.45,3.41,3.38 (s, 18H). ^{31}P NMR (CD_2Cl_2) δ/ppm: 11.5(m, 1P, J_{Pt-P} = 2430 Hz, J_{P-P} = 35.8 Hz), 4.0 (m, 2P, J_{Ag-P} = 521 Hz, J_{P-P} = 36.7 Hz).

$[PtAg_2(dpmp)_2(C{\equiv}Cbph\text{-}4)_2](ClO_4)_2$ (10). This compound was prepared by the same synthetic procedure as that of **1** except for the use of 4-ethynylbiphenyl instead of phenylacetylene. Yield: 86%. Anal. Calcd for $C_{92}H_{76}Ag_2Cl_2O_8P_6Pt$: C, 55.89; H, 3.87. Found: C, 55.94; H, 3.90. ESI-MS m/z (%): 1877.3 (100) $[M-ClO_4]^+$. IR (KBr) ν/cm^{-1}: 2099w (C≡C), 1096s (ClO_4). ^{1}H NMR (DMSO) δ/ppm: 7.94−7.84 (m, 4H), 7.68−7.52 (m, 20H), 7.52−7.38 (m, 13H), 7.35−7.21 (m, 14H), 7.20−7.12 (m 7H), 7.12−7.04 (t, 3H, J = 7.5 Hz), 6.83−6.76(t, 3H, J = 7.4 Hz), 6.68−6.62 (d, 2H, J = 8.0 Hz), 6.56−6.49 (d, 2H, J = 8.1 Hz), 4.52−4.36 (m, 4H), 3.78−3.66 (m, 4H). ^{31}P NMR (DMSO) δ/ppm: 14.63(m, 1P, J_{Pt-P} = 2551 Hz, J_{P-P} = 46.8 Hz), −5.17 (m, 2P, J_{Ag-P} = 460 Hz, J_{P-P} = 41.7 Hz).

$[PtAg_2(dpmp)_2(C{\equiv}Cphen\text{-}9)_2](ClO_4)_2$ (11). This compound was prepared by the same synthetic procedure as that of **1** except for the use of 9-ethynyl-phenanthrene instead of phenylacetylene. Yield: 86%. Anal. Calcd for $C_{96}H_{76}Ag_2Cl_2O_8P_6Pt$: C, 56.93; H, 3.78. Found: C, 56.99; H, 3.85. ESI-MS m/z (%): 1925.7 (100) $[M-ClO_4]^+$. IR (KBr) ν/cm^{-1}: 2093w (C≡C), 1097s (ClO_4). ^{1}HNMR (DMSO) δ/ppm: 8.79−8.72 (m, 4H), 7.89−7.79 (m, 5H), 7.72−7.42 (m, 27H), 7.41−7.35 (t, 4H, J = 7.4 Hz), 7.34−7.26 (m, 2H), 7.26−7.11 (m,18H), 6.93−6.88(m, 1H), 6.85−6.68 (t, 4H, J = 7.7 Hz), 6.53, 6.42 (s, 2H), 6.30−6.24 (t, 1H, J = 7.6 Hz), 4.72−4.50 (m, 4H), 3.83−3.69 (m,

dx.doi.org/10.1021/ic4000457 | Inorg. Chem. 2013, 52, 5167−5175

4H). ^{31}P NMR (DMSO) δ/ppm: 16.60 (m, 1P, J_{Pt-P} = 2536 Hz, J_{P-P} = 41.9 Hz), −5.02 (m, 2P, J_{Ag-P} = 480 Hz, J_{P-P} = 42.3 Hz).

$[PtAg_2(dpmp)_2(C{\equiv}Cpyr\text{-}4)_2](ClO_4)_2$ (12). This compound was prepared by the same synthetic procedure as that of **1** except for the use of 4-ethynyl-pyrene instead of phenylacetylene. Yield: 86%. Anal. Calcd for $C_{100}H_{76}Ag_2Cl_2O_8P_6Pt{\cdot}H_2O$: C, 57.43; H, 3.76. Found: C, 57.35; H, 3.83. ESI-MS m/z (%): 1973.0 (100) $[M\text{-}ClO_4]^+$. IR (KBr) ν/cm^{-1}: 2082w (C≡C), 1096s (ClO_4). ^{1}H NMR (DMSO) δ/ppm: 8.34−8.23 (m, 3H), 8.20−8.05 (m, 7H), 8.02−7.80 (m, 8H), 7.70−7.55 (m, 15H), 7.52−7.34 (m, 12H), 7.31−7.12 (m,17H), 6.88−6.80(t, 4H, J = 7.6 Hz), 6.75−6.67 (m, 2H), 4.70−4.46 (m, 4H), 3.89−3.71 (m, 4H). ^{31}P NMR (DMSO) δ/ppm: 16.28(m, 1P, J_{Pt-P} = 2530 Hz, J_{P-P} = 41.7 Hz), −5.00 (m, 2P, J_{Ag-P} = 493 Hz, J_{P-P} = 42.0 Hz).

Physical Measurements. UV−vis absorption spectra were measured on a Perkin-Elmer Lambda 25 UV−vis spectrophotometer. Infrared spectra (IR) were recorded on a Magna 750 FT-IR spectrophotometer with KBr pellets. Elemental analysis (C, H, N) were carried out on a Perkin-Elmer model 240 C elemental analyzer. Electrospray ionization mass spectrometry (ESI-MS) was performed on a Finnigan LCQ mass spectrometer using dichloromethane and methanol mixtures as mobile phases. ^{1}H and ^{31}P NMR spectra were recorded on a Bruker Avance III 400 spectrometer with $SiMe_4$ and H_3PO_4 as internal and external references, respectively. Emission and excitation spectra were recorded on a Perkin-Elmer LS55 luminescence spectrometer with a red-sensitive photomultiplier type R928. Emission lifetimes in solid states and degassed solutions were determined on an Edinburgh analytical instrument (F900 fluorescence spectrometer). The emission quantum yield (Φ_{em}) in degassed dichloromethane solution at room temperature was calculated by $\Phi_s = \Phi_r(B_r/B_s)(n_s/n_r)^2(D_s/D_r)$ using $[Ru(bpy)_3](PF_6)_2$ in acetonitrile as the standard (Φ_{em} = 0.062) for the samples,[32] where the subscripts r and s denote reference standard and the sample solution, respectively, and n, D, and Φ are the refractive index of the solvents, the integrated intensity, and the luminscence quantum yield, respectively. The quantity B is calculated by $B = 1-10^{-AL}$, where A is the absorbance at the excitation wavelength and L is the optical path length. Solid-state quantum yields of powder samples in sealed quartz cuvettes were determined by the integrating sphere using a SHIMADZU RF-5301PC spectrofluorophotometer. To probe selectivity and reversibility of the vapochromic properties to specific solvents, concentrated CH_2Cl_2 solutions were put on quartz disks which were purged with N_2 to dry. Luminescence vapochromic experiments were performed upon sufficient exposure of the quartz disks or crystals to various saturated vapors at ambient temperature for 10−15 min. A rapid vapochromic response is usually observed in dozens of seconds to several minutes depending on sample thickness in quartz disks or size of the crystals. The PMMA films were made on quartz slides (2.5 cm × 4 cm) using spin coating method, in which the solution was prepared by dissolving complex **9** (10 mg) and PMMA (polymethylmethacrylate, 40 mg) in dichloromethane (2 mL).

Crystal Structural Determination. Crystals suitable for X-ray crystallographic measurement were grown by layering diethyl ether, *n*-hexane, or *n*-heptane onto corresponding solutions with coordination or/and crystal solvents, respectively, including **1**·2CH_2Cl_2, **2**·CH_2Cl_2, **4**·4CH_2Cl_2, **4**(MeCN)·MeCN, **5**·2CH_2Cl_2·2H_2O, **5**$(py)_2$·2py, **9**·2acetone, **9**$(DMF)_2$·2DMF, **9**$(MeCN)_2$·2Et_2O, and **9**$(py)_2$·2py. Data collection was performed on Mercury CCD diffractometer by the ω scan technique at room temperature using graphite-monochromated Mo−Kα (λ = 0.71073 Å) radiation. The CrystalClear software package was used for data reduction and empirical absorption correction. The structures were solved by direct methods. The heavy atoms were located from E-map, and the rest of the non-hydrogen atoms were found in subsequent Fourier maps. All non-hydrogen atoms were refined anisotropically, while the hydrogen atoms were generated geometrically and refined with isotropic thermal parameters. The structures were refined on F^2 by full-matrix least-squares methods using the *SHELXTL*-97 program package.[33] For **1**·2CH_2Cl_2 and **2**·CH_2Cl_2, the solvate molecules were treated as a diffuse contribution to the overall scattering without specific atom positions by SQUEEZE/PLATON due to severe disorder of these solvate molecules in the lattices.

Computational Methodology. To understand the electronic and spectroscopic properties as well as the nature of absorption and emission origins, computational studies on **1** were implemented using Gaussian 03 program package.[34] First, the density functional theory (DFT)[35] method at the gradient-corrected correlation functional PBE1PBE[36] level was used to optimize the geometrical structures. The initial structure was extracted from the experimentally determined geometries obtained from the X-ray crystallographic data. Then, a hundred of singlet and six triplet excited states were calculated by the TD-DFT method[37] at the PBE1PBE level based on the optimized gas-phase structures. In the calculations of excited states, the conductor-like polarizable continuum model method (CPCM)[38] considering the solvent effects of CH_2Cl_2 was employed. To compare the electronic structures of complexes **5**·2CH_2Cl_2·2H_2O and **5**$(py)_2$·2py, the crystal structures without further geometrical optimization were used for excited-state calculations. The Pt−M interactions were also estimated by the Mayer bond order.[39] In these calculations, the Lanl2dz effective core potential was used to describe the inner electrons of Pt, Ag, and P atoms,[40] while the associated double-ζ basis set of Hay and Wadt was employed for the remaining outer electrons. Other nonmetal atoms of C, H, O, and N were described by all-electron basis set of 6-31G(p,d).[41] To precisely describe the electronic properties, one additional f-type polarization function was used for Pt (α_f = 0.18) and Ag (α_f = 0.22) atoms, and an extra d-type polarization function was added in P (α_d = 0.34) atoms.[42]

■ ASSOCIATED CONTENT

Ⓢ Supporting Information

Tables and figures giving additional photophysical and computational results, and X-ray crystallographic files in CIF format for the determination of 10 structures. This material is available free of charge via the Internet at http://pubs.acs.org.

■ AUTHOR INFORMATION

Corresponding Author

*E-mail: czn@fjirsm.ac.cn.

Notes

The authors declare no competing financial interest.

■ ACKNOWLEDGMENTS

We are grateful for financial support from the NSFC (20931006, U0934003, and 91122006) and the NSF of Fujian Province (2011J01065).

■ REFERENCES

(1) (a) Williams, J. A. G. *Top Curr. Chem.* **2007**, *281*, 205. (b) Rausch, A. F.; Homeier, H. H. H.; Yersin, H. *Top Organomet. Chem.* **2010**, *29*, 193. (c) Muro, M. L.; Rachford, A. A.; Wang, X.; Castellano, F. N. *Top Organomet. Chem.* **2010**, *29*, 159.

(2) (a) Yam, V. W.-W.; Cheng, E. C.-C. *Top Curr. Chem.* **2007**, *281*, 269. (b) Lima, J. C.; Rodriguez, L. *Chem. Soc. Rev.* **2011**, *40*, 5442.

(3) Sculfort, S.; Braunstein, P. *Chem. Soc. Rev.* **2011**, *40*, 2741.

(4) (a) Berenguer, J. R.; Lalinde, E.; Moreno, M. T. *Coord. Chem. Rev.* **2010**, *254*, 832. (b) Díez, Á.; Lalinde, E.; Moreno, M. T. *Coord. Chem. Rev.* **2011**, *255*, 2426.

(5) (a) Buschbecka, R.; Lowb, P. J.; Lang, H. *Coord. Chem. Rev.* **2011**, *255*, 241. (b) Lang, H.; del Villar, A.; Stein, T.; Zoufala, P.; Ruffer, T.; Rheinwald, G. *J. Organomet. Chem.* **2007**, *692*, 5203.

(6) Wong, W.-Y.; Lu, G. L.; Choi, K.-H. *J. Organomet. Chem.* **2002**, *659*, 107.

(7) (a) Phillips, V.; Willard, K. J.; Golen, J. A.; Moore, C. J.; Rheingold, A. L.; Doerrer, L. H. *Inorg. Chem.* **2010**, *49*, 9265. (b) Adams, C. J.; Fey, N.; Harrison, Z.; Sazanovich, I. V.; Tow-rie, M.; Weinstein, J. A. *Inorg. Chem.* **2008**, *47*, 8242.

(8) (a) Charmant, J. P. H.; Forniés, J.; Gómez, J.; Lalinde, E.; Merino, R. I.; Moreno, M. T.; Orpen, A. G. *Organometallics* **1999**, *18*, 3353. (b) Ara, I.; Forniés, J.; Gómez, J.; Lalinde, E.; Moreno, M. T. *Organometallics* **2000**, *19*, 3137. (c) Gil, B.; Fornies, J.; Gomez, J.; Lalinde, E.; Martn, A.; Moreno, M. T. *Inorg. Chem.* **2006**, *45*, 7788.
(9) (a) Yam, V. W.-W.; Yu, K.-L.; Wong, K. M.-C.; Cheung, K.-K. *Organometallics* **2001**, *20*, 721. (b) Yam, V. W.-W.; Hui, C.-K.; Wong, K. M.-C.; Zhu, N.; Cheung, K.-K. *Organometallics* **2002**, *21*, 4326. (c) Leung, S. Y.-L.; Lam, W. H.; Zhu, N.; Yam, V. W.-W. *Organometallics* **2010**, *29*, 5558. (d) Yam, V. W.-W.; Hui, C.-K.; Yu, S.-Y.; Zhu, N. *Inorg. Chem.* **2004**, *43*, 812. (e) Yam, V. W.-W.; Chan, L.-P.; Lai, T.-F. *J. Chem. Soc., Dalton Trans.* **1993**, 2075.
(10) (a) Chen, Z.-N.; Zhao, N.; Fan, Y.; Ni, J. *Coord. Chem. Rev.* **2009**, *253*, 1. (b) Wei, Q.-H.; Yin, G.-Q.; Ma, Z.; Shi, L.-X.; Chen, Z.-N. *Chem. Commun.* **2003**, 2188. (c) Yin, G.-Q.; Wei, Q.-H.; Zhang, L.-Y.; Chen, Z.-N. *Organometallics* **2006**, *25*, 580.
(11) (a) Umakoshi, K.; Saito, K.; Arikawa, Y.; Onishi, M.; Ishizaka, S.; Kitamura, N.; Nakao, Y.; Sakaki, S. *Chem.—Eur. J.* **2009**, *15*, 4238. (b) Umakoshi, K.; Kojima, T.; Saito, K.; Akatsu, S.; Onishi, M.; Ishizaka, S.; Kitamura, N.; Nakao, Y.; Sakaki, S.; Ozawa, Y. *Inorg. Chem.* **2008**, *47*, 5033. (c) Fuertes, S.; Woodall, C. H.; Raithby, P. R.; Sicilia, V. *Organometallic* **2012**, *31*, 4228. (d) Julia, F.; Jones, P. G.; Gonzalez-Herrero, P. *Inorg. Chem.* **2012**, *51*, 5037.
(12) (a) ManojloviC-Muir, L.; Muir, K. W.; Treurnicht, I.; Puddephatt, R. J. *Inorg. Chem.* **1987**, *26*, 2418. (b) Manojlovi-Muir, L.; Henderson, A. N.; Treurnicht, I.; Puddephatt, R. J. *Organometallics* **1989**, *8*, 2055.
(13) (a) Mohr, F.; Mendia, A.; Laguna, M. *Eur. J. Inorg. Chem.* **2007**, 3115. (b) Casas, J. M.; Fornies, J.; Fuertes, S.; Martin, A.; Sicilia, V. *Organometallics* **2007**, *26*, 1674. (c) Fornies, J.; Fuertes, S.; Martin, A.; Sicilia, V.; Lalinde, E.; Moreno, M. T. *Chem.—Eur. J.* **2006**, *12*, 8253.
(14) Yip, J. H. K.; Wu, J.; Wong, K.-Y.; Ho, K. P.; Pun, C. S.-N.; Vittal, J. J. *Organometallics* **2002**, *21*, 5292.
(15) (a) Vicente, J.; Chicote, M.-T.; Alvarez-Falcon, M. M. *Organometallics* **2005**, *24*, 2764. (b) Vicente, J.; Chicote, M.-T.; Alvarez-Falcon, M. M.; Jones, P. G. *Chem. Commun.* **2004**, 2658.
(16) Whiteford, J. A.; Stang, P. J.; Huang, S. D. *Inorg. Chem.* **1998**, *37*, 5595.
(17) (a) Lang, H.; Zoufala, P.; Klaib, S.; del Villar, A.; Rheinwald, G. *J. Organomet. Chem.* **2007**, *692*, 4168. (b) Lang, H.; Packheiser, R.; Walfort, B. *Organometallics* **2006**, *25*, 1836.
(18) (a) Bruce, M. I.; Costuas, K.; Halet, J.-F.; Hall, B. C.; Low, P. J.; Nicholson, B. K.; Skelton, B. W.; White, A. H. *J. Chem. Soc., Dalton Trans.* **2002**, 383. (b) Li, Q.-S.; Xu, F.-B.; Cui, D.-J.; Yu, K.; Zeng, X.-S.; Leng, X.-B.; Song, H.-B.; Zhang, Z.-Z. *Dalton Trans.* **2003**, 1551.
(19) McDonald, W. S.; Pringle, P. G.; Shaw, B. L. *Chem. Commun.* **1982**, 861.
(20) Yip, H.-K.; Lin, H.-M.; Wang, Y.; Che, C.-M. *J. Chem. Soc., Dalton Trans.* **1993**, 2939.
(21) Schmittel, M.; Kalsani, V.; Bats, J. W. *Inorg. Chem.* **2005**, *44*, 4115.
(22) (a) Yamazaki, S.; Deeming, A. J.; Speel, D. M.; Hibbs, D. E.; Hursthouse, M. B.; Malik, K. M. A. *Chem. Commun.* **1997**, 177. (b) Yamazaki, S.; Deeming, A. J. *J. Chem. Soc., Dalton Trans.* **1993**, 3051.
(23) (a) Quadras, L. de; Shelton, A. H.; Kuhn, H.; Hampel, F.; Schanze, K. S.; Gladysz, J. A. *Organometallics* **2008**, *27*, 4979. (b) Fortin, D.; Clement, S.; Gagnon, K.; Berube, J.-F.; Stewart, M. P.; Geiger, W. E.; Harvey, P. D. *Inorg. Chem.* **2009**, *48*, 446.
(24) Ara, I.; Fornies, J.; Lalinda, E.; Moreno, M. T.; Tomas, M. *J. Chem. Soc., Dalton Trans.* **1995**, 2397.
(25) Che, C.-M.; Yip, H.-K.; Li, D.; Peng, S.-M.; Lee, G.-H.; Wang, Y.-M.; Liu, S.-T. *Chem. Commun.* **1991**, 1615.
(26) (a) Takemura, Y.; Nakajima, T.; Tanaase, T. *Eur. J. Inorg. Chem.* **2009**, 4820. (b) Tanase, T.; Toda, H.; Yamamoto, Y. *Inorg. Chem.* **1997**, *36*, 1571.
(27) (a) Zhang, X.; Li, B.; Chen, Z.-H.; Chen, Z.-N. *J. Mater. Chem.* **2012**, *22*, 11427. (b) Wenger, O. S. *Chem. Rev.* **2013**, DOI: 10.1021/cr300396p. (c) Kato, M. *Bull. Chem. Soc. Jpn.* **2007**, *80*, 287−294.
(28) (a) Mansour, M. A.; Connick, W. B.; Lachicotte, R. J.; Gysling, H. J.; Eisenberg, R. *J. Am. Chem. Soc.* **1998**, *120*, 1329. (b) Lim, S. H.; Olmstead, M. M.; Balch, A. L. *J. Am. Chem. Soc.* **2011**, *133*, 10229. (c) Muro, M. L.; Daws, C. A.; Castellano, F. N. *Chem. Commun.* **2008**, 6134. (d) Hudson, Z. M.; Sun, C.; Harris, K. J.; Lucier, B. E. G.; Schurko, R. W.; Wang, S. *Inorg. Chem.* **2011**, *50*, 3447. (e) Li, Y.-J.; Deng, Z.-Y.; Xu, X.-F.; Wu, H.-B.; Cao, Z.-X.; Wang, Q.-M. *Chem. Commun.* **2011**, *47*, 9179.
(29) (a) Fernandez, E. J.; Lopez-de-Luzuriaga, J. M.; Monge, M.; Montiel, M.; Olmos, M. E.; Perez, J.; Laguna, A.; Mendizabal, F.; Mohamed, A. A.; Fackler, J. P., Jr. *Inorg. Chem.* **2004**, *43*, 3573. (b) Laguna, A.; Lasanta, T.; Lopez-de-Luzuriaga, J. M.; Monge, M.; Naumov, P.; Olmos, M. E. *J. Am. Chem. Soc.* **2010**, *132*, 456.
(30) Strasser, C. E.; Catalano, V. J. *J. Am. Chem. Soc.* **2010**, *132*, 10009.
(31) Appel, R.; Geisler, K.; Scholer, H.-F. *Chem. Ber.* **1979**, *112*, 648−653.
(32) Demasa, J. N.; Crosby, G. A. *J. Phys. Chem.* **1971**, *75*, 991−1024.
(33) Sheldrick, G. M. *SHELXL-97, Program for the Refinement of Crystal Structures*; University of Göttingen: Göttingen, Germany, 1997.
(34) Frisch, M. J.; Trucks, G. W.; Schlegel, H. B.; Scuseria, G. E.; Robb, M. A.; Cheeseman, J. R.; Montgomery, J. A.; Jr.; Vreven, T.; Kudin, K. N.; Burant, J. C.; Millam, J. M.; Iyengar, S. S.; Tomasi, J.; Barone, V.; Mennucci, B.; Cossi, M.; Scalmani, G.; Rega, N.; Petersson, G. A.; Nakatsuji, H.; Hada, M.; Ehara, M.; Toyota, K.; Fukuda, R.; Hasegawa, J.; Ishida, M.; Nakajima, T.; Honda, Y.; Kitao, O.; Nakai, H.; Klene, M.; Li, X.; Knox, J. E.; Hratchian, H. P.; Cross, J. B.; Bakken, V.; Adamo, C.; Jaramillo, J.; Gomperts, R.; Stratmann, R. E.; Yazyev, O.; Austin, A. J.; Cammi, R.; Pomelli, C.; Ochterski, J. W.; Ayala, P. Y.; Morokuma, K.; Voth, G. A.; Salvador, P.; Dannenberg, J. J.; Zakrzewski, V. G.; Dapprich, S.; Daniels, A. D.; Strain, M. C.; Farkas, O.; Malick, D. K.; Rabuck, A. D.; Raghavachari, K.; Foresman, J. B.; Ortiz, J. V.; Cui, Q.; Baboul, A. G.; Clifford, S.; Cioslowski, J.; Stefanov, B. B.; Liu, G.; Liashenko, A.; Piskorz, P.; Komaromi, I.; Martin, R. L.; Fox, D. J.; Keith, T.; Al-Laham, M. A.; Peng, C. Y.; Nanayakkara, A.; Challacombe, M.; Gill, P. M. W.; Johnson, B.; Chen, W.; Wong, M. W.; Gonzalez, C.; Pople, J. A. *Gaussian 03, revision D.02*; Gaussian, Inc.: Wallingford, CT, 2004.
(35) Becke, A. D. *J. Chem. Phys.* **1993**, *98*, 5648−5652.
(36) Perdew, J. P.; Burke, K.; Ernzerhof, M. *Phys. Rev. Lett.* **1996**, *77*, 3865−3868.
(37) (a) Bauernschmitt, R.; Ahlrichs, R. *Chem. Phys. Lett.* **1996**, *256*, 454−464. (b) Casida, M. E.; Jamorski, C.; Casida, K. C.; Salahub, D. R. *J. Chem. Phys.* **1998**, *108*, 4439−4449.
(38) Cossi, M.; Rega, N.; Scalmani, G.; Barone, V. *J. Comput. Chem.* **2003**, *24*, 669−681.
(39) Mayer, I. *Chem. Phys. Lett.* **1983**, *97*, 270−274.
(40) (a) Hay, P. J.; Wadt, W. R. *J. Chem. Phys.* **1985**, *82*, 270−283. (b) Wadt, W. R.; Hay, P. J. *J. Chem. Phys.* **1985**, *82*, 284−298. (c) Hay, P. J.; Wadt, W. R. *J. Chem. Phys.* **1985**, *82*, 299−310.
(41) Francl, M. M.; Pietro, W. J.; Hehre, W. J.; Binkley, J. S.; Gordon, M. S.; DeFrees, D. J.; Pople, J. A. *J. Chem. Phys.* **1982**, *77*, 3654−3665.
(42) Pyykkő, P.; Runeberg, N.; Mendizabal, F. *Chem.—Eur. J.* **1997**, *3*, 1451−1457.